

Bright Optical Eigenmode of 1 nm³ Mode VolumeWancong Li,^{1,2} Qiang Zhou,^{1,2} Pu Zhang^{1,2,*} and Xue-Wen Chen^{1,2,†}¹*School of Physics and Wuhan National Laboratory for Optoelectronics, Huazhong University of Science and Technology, Luoyu Road 1037, Wuhan, 430074, People's Republic of China*²*Institute for Quantum Science and Engineering, Huazhong University of Science and Technology, Luoyu Road 1037, Wuhan 430074, People's Republic of China*

(Received 6 January 2021; accepted 26 May 2021; published 25 June 2021)

We report on the discovery and rationale to devise bright single optical eigenmodes that feature quantum-optical mode volumes of about 1 nm³. Our findings rely on the development and application of a quasinormal mode theory that self-consistently treats fields and electron nonlocality, spill-out, and Landau damping around atomistic protrusions on a metallic nanoantenna. By outpacing Landau damping with radiation via properly designed antenna modes, the extremely localized modes become bright with radiation efficiencies reaching 30% and could provide up to 4×10^7 times intensity enhancement.

DOI: [10.1103/PhysRevLett.126.257401](https://doi.org/10.1103/PhysRevLett.126.257401)

Confining light in an eigenmode with a tiny volume is fundamentally important and underpins new technologies. Over the past several decades, metal (plasmonic) nanostructures have been widely pursued for concentrating light into volumes that are well below diffraction limit [1–3]. The shrinkage is due to the mixing of fields and surface electrons, for instance, resonantly in terms of optical antennas and nanocavities [4,5] or nonresonantly through lightning rod effect [6,7], and so on. With resonant and nonresonant effects combined [2,8], ultrathin metallic gaps have been employed to further enhance light concentration [9–13]. Moreover, researchers have investigated both experimentally [14,15] and theoretically [16–18] the inclusion of atomistic protrusions in an ultrathin gap for extreme field localization. The protrusions may naturally occur [17,19] or be assembled onto a host nanoparticle via nanomanipulation [15]. Experiments have demonstrated subnanometer-resolution optical imaging with huge signal enhancement, including Raman scattering [20,21] and single-molecule photoluminescence [15]. The underlying physics is, however, still elusive. The contribution of the atomistic protrusion has been recognized as the nonresonant lightning rod effect. Landau damping (LD), which accounts for single-electron excitation by large-wavenumber field components [22,23] and is often omitted, induces severe loss and may diminish the lightning rod effect.

In a broader perspective, an intriguing question is whether it is possible to have optical eigenmodes with similar scale of electron wave function in a photon emitter. To this end, a rigorous modal analysis of the extremely localized field is indispensable for understanding the mode structure and exploring the boundary of localization. Moreover, instead of a geometrical estimation, it enables the use of the quantum optically defined mode volume to quantify the field localization [24–26]. The inherent

openness and material absorption of the system requires a modal analysis in the framework of quasinormal modes (QNMs) [27–29]. However, existing QNM theories [27–31] cannot be applied since the nanostructures of interest possess a relatively large host (~ 100 nm) and tiny protrusions that are expected to exhibit significant quantum and many-body effects, such as nonlocal response [10,32], LD [22], and electron spillover [33]. Although *ab initio* methods or time-dependent density functional theory (TD-DFT) can correctly describe these effects [16,34], they become computationally intractable for nanoparticles larger than a few nanometers. Quantum hydrodynamic models (QHDMs) with recent new developments can self-consistently describe the aforementioned microscopic details of a macroscopic system in a computationally efficient manner [33,35,36]. Notably, results from QHDMs agree well with TD-DFT calculations and can reproduce the size-dependent damping rate due to LD for metal nanospheres down to 1 nm in diameter [36].

Here, by developing a QHDM-based QNM theory, we report on the discovery, characterization, and engineering of optical eigenmodes with mode volumes about 1 nm³ (smallest to 0.5 nm³). Such extremely localized mode (ELM) originates from resonant accumulation of conduction electrons around the atomistic protrusion and the resulting mode volume is about 2 orders of magnitude smaller than the gap-plasmon mode enhanced by the nonresonant lightning rod effect. Moreover, we present a strategy to reconcile the longstanding dilemma of extreme localization and efficient radiation to make the ELMs bright. Our findings put photons and photon emitters on equal footing and venture into a new regime of optical physics.

In QHDM, the conduction electrons in metal are characterized by the number density $n(\mathbf{r}, t)$ and velocity $\mathbf{v}(\mathbf{r}, t)$. Assuming weak light excitation, the response can be treated

perturbatively, i.e., $n = n_0 + n_1$, where n_0 is the stationary part in absence of light excitation and n_1 is the small light-induced dynamic part. The polarization field \mathbf{P} is related to n_1 as $n_1 = -\nabla \cdot \mathbf{P}/q_e$ and the current density \mathbf{J} reads as $\mathbf{J} \approx n_0 q_e \mathbf{v}$ with q_e being the electron charge. Under the perturbative treatment, a linearized hydrodynamic equation can be obtained in the frequency domain as

$$i\tilde{\omega}\mathbf{J} = -\gamma_D\mathbf{J} + \frac{q_e n_0}{m_e} \left[q_e \mathbf{E} - \nabla \left(\frac{\delta G}{\delta n} \right)_1 + \frac{\nabla \cdot \bar{\sigma}}{n_0} \right], \quad (1)$$

where m_e and γ_D denote the electron mass and decay rate, respectively. The second term in the bracket includes the internal energy functional of the electron liquid $G = \int d\mathbf{r} g(n)$ [35]. The energy density $g(n) = T_{\text{TF}} + T_w + e_{\text{XC}}$ consists of Thomas-Fermi kinetic energy T_{TF} , von Weizsäcker kinetic energy T_w , and exchange correlation e_{XC} . Here $(\dots)_1$ means taking the terms linear to n_1 . $\bar{\sigma}$ is the viscous stress tensor related to \mathbf{v} and describes LD [36]. The light-driven current couples with the optical fields as

$$i\tilde{\omega}\varepsilon_b \mathbf{E} = \nabla \times \mathbf{H} - \mathbf{J}. \quad (2)$$

Here ε_b is the background permittivity of metal, which could include contribution from bound electrons. Equations (1) and (2), $i\tilde{\omega}\mathbf{P} = \mathbf{J}$ and $i\tilde{\omega}\mu\mathbf{H} = -\nabla \times \mathbf{E}$ can be formulated into a linear eigenvalue problem as $M[\mathbf{E}, \mathbf{H}, \mathbf{J}, \mathbf{P}]^T = \tilde{\omega}[\mathbf{E}, \mathbf{H}, \mathbf{J}, \mathbf{P}]^T$, where M is a frequency-independent operator and $\tilde{\omega}$ is a complex eigenvalue. A detailed derivation of the QHDM-based QNM theory is given in the Supplemental Material [37].

The QHDM and QNM calculations are performed with the finite element method using a multiscale meshing scheme. We employ an iterative procedure to locate the complex frequency poles $\tilde{\omega}_q = \omega_q + i\gamma_q$ and use an integration-free approach [53] to normalize the corresponding mode profiles $\tilde{\mathbf{E}}_q$, where q is a mode index. According to the universal definition [26,30,54], the position-dependent complex mode volume of a QNM reads

$$\tilde{V}_q(\mathbf{r}) = 1/[n_d^2(\mathbf{r})\tilde{\mathbf{E}}_q^2(\mathbf{r})], \quad (3)$$

where $n_d(\mathbf{r})$ is refractive index. We characterize the level of mode confinement by the minimum volume $\tilde{V}_m = \tilde{V}_q(\mathbf{r})|\tilde{\mathbf{E}}_q(\mathbf{r})/\tilde{\mathbf{E}}_q(\mathbf{r}_M)|^2$, where $|\tilde{\mathbf{E}}_q(\mathbf{r}_M)|$ is the maximum field. Complex mode volume is well known to have a general analytical relation with the QNM's modal contribution $f_{P,q}$ to Purcell factor spectrum [27,30,37,55]. Here, to independently obtain $f_{P,q}$, a dipole source \mathbf{J}_s is applied to excite the system. By following the Riesz projection procedure [56], the resulting electric field at the source position is expanded as $\mathbf{E}(\omega) = \sum_q \mathbf{E}_q(\omega) + \mathbf{E}_{\text{nr}}$, where the sum accounts for the contributions of all involved QNMs and \mathbf{E}_{nr} is the remaining nonresonant contribution.

Then one obtains $f_{P,q} = -\frac{1}{2}\text{Re}[\mathbf{E}_q(\omega_q) \cdot \mathbf{J}_s^*]/P_0$ where P_0 is the radiation power of \mathbf{J}_s in vacuum. We confirm $f_{P,q}$ obtained by the analytical and numerical methods match perfectly [37].

We start with a simple structure shown in Fig. 1(a), i.e., a gold nanoparticle (host) with a cone-shaped atomistic protrusion, which has a fixed base diameter $D_p = 1.2$ nm and a varying height h_p . To pinpoint the modal properties, a vertically oriented dipole placed 0.5 nm below the protrusion tip is used to excite the system. Such setting is used throughout the Letter and the details for the numerical

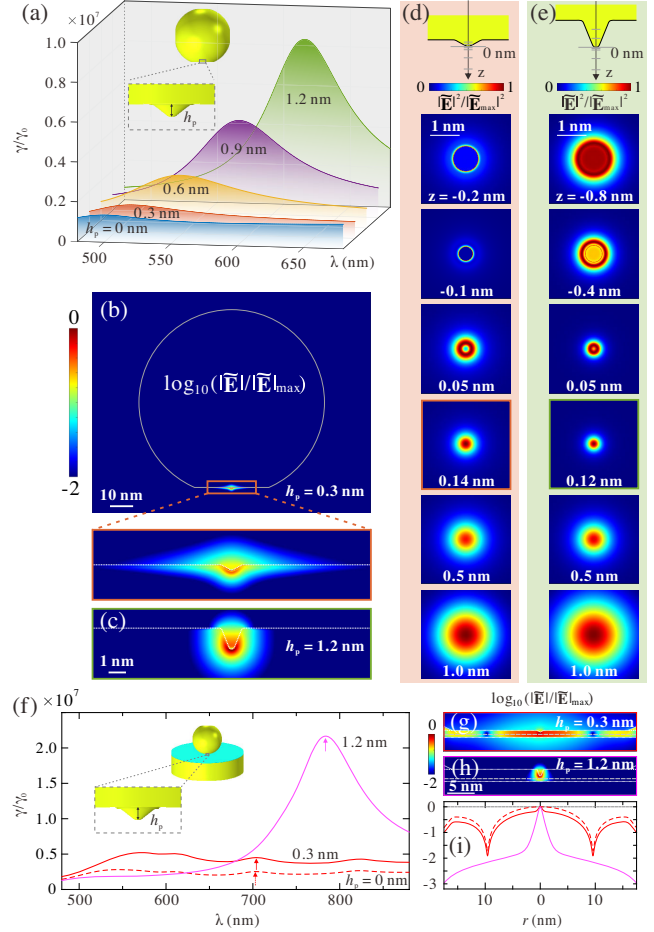


FIG. 1. (a) Emission enhancement spectra for a dipole placed 0.5 nm below a cone-shaped protrusion with a varying height. The host is an 80 nm diameter gold nanosphere with a 32 nm diameter flat bottom. (b) ELM field profile in logarithmic scale for $h_p = 0.3$ nm. (c) ELM field profile near the protrusion for $h_p = 1.2$ nm. (d),(e) Normalized intensity distributions at various vertical distances from the tip for $h_p = 0.3$ and 1.2 nm, respectively. (f) Emission enhancement spectra for the dipole in three NPoM structures of different dielectric gaps and protrusion heights: ($d = 1.3, h_p = 0$), ($d = 1.3, h_p = 0.3$), and ($d = 2.2, h_p = 1.2$) nm. The dielectric has a refractive index of 1.45. (g),(h) Mode profiles in the gap for the resonances denoted by the arrows in (f). (i) Electric fields along the line 0.5 nm above the substrate for the three indicated modes.

implementation (geometry parameters, material, meshing, etc.) are provided in the Supplemental Material [37]. The color-coded traces in Fig. 1(a) plot the spectra of emission enhancement. With the introduction of the protrusion, a prominent resonance appears and redshifts as the protrusion height increases. The huge enhancement peaks (approaching 10^7) imply the existence of a class of ELMs, whose resonant wavelength does not depend on the host nanoparticle but instead on the protrusion shape. These observations are confirmed by rigorous QHDM-based QNM calculations. For the case with the bluntest protrusion ($h_p = 0.3$ nm), we find a complex wavelength pole at $\tilde{\lambda} = 489 - 43i$ nm contributing the majority ($\sim 80\%$) of the emission enhancement. Figure 1(b) displays the mode profile in logarithmic scale. An enlarged view in the lower panel depicts the modal field localized near the protrusion. Protrusions with different heights all support such modes [37] and Fig. 1(c) depicts the ELM for $h_p = 1.2$ nm. Fine features of the mode profiles are revealed by showing the normalized intensity distribution at various vertical distances from the protrusion tip in Figs. 1(d) and 1(e) for $h_p = 0.3$ and 1.2 nm, respectively. Outside the metal, the smallest spot sizes (full widths at half maximum) are 0.54 nm at $z = 0.14$ nm for $h_p = 0.3$ nm, and 0.38 nm at $z = 0.12$ nm for 1.2 nm, respectively. Our calculations show \tilde{V}_m of $2.0 - 1.5i$, $1.0 - 0.24i$, $0.69 - 0.018i$, and $0.58 + 0.033i$ nm³ for $h_p = 0.3, 0.6, 0.9,$ and 1.2 nm, respectively.

Having demonstrated the existence of ELMs on a stand-alone nanoparticle, we examine the nanoparticle-on-mirror (NPoM) structure that has recently attracted considerable interest [10–12,14]. The enhancement spectra shown in Fig. 1(f) correspond to the cases of no protrusion, with protrusions of $h_p = 0.3$ and 1.2 nm, respectively. The first two spectra are quite flat because of the LD effect [22], revealing the necessity of taking LD into account in the model (spectra without considering LD are plotted in Fig. S1 in the Supplemental Material [37]). Nevertheless, there is a recognizable resonance around 700 nm for $h_p = 0.3$ nm (indicated by an arrow) and it is called the “picocavity” mode [14]. This mode is essentially the quadrupolar gap-plasmon resonance similar to the case without the protrusion. For $h_p = 1.2$ nm, the situation is very different and there exists a huge enhancement peak around 780 nm. The corresponding mode profiles for $h_p = 0.3$ and 1.2 nm near the protrusion are displayed in logarithmic scale in Figs. 1(g) and 1(h), respectively. Figure 1(i) plots the field profiles along the line 0.5 nm above the substrate for all three cases. The field profile for $h_p = 0.3$ nm largely follows the profile of the no-protrusion case and exhibits a small bump that is due to the lightning rod effect from the protrusion. In contrast, the mode field for $h_p = 1.2$ nm is clearly much more localized. The calculated mode volumes are $310 - 14i, 74 - 16i,$ and

$0.43 - 0.017i$ nm³ for the no-protrusion, $h_p = 0.3$ (picocavity), and 1.2 nm cases, respectively. Here one sees the great difference in concentrating the field between the nonresonant lightning rod effect and the resonance effect of the protrusion.

Next we expound the formation mechanism of ELMs with methods at different levels of approximation in treating metal, namely, the classical local response approximation (LRA), the hard-wall hydrodynamic model [30] (HW-HDM), and QHDM with and without LD correction. Taking $h_p = 1.2$ nm in Fig. 1(a) as the example, we display the calculated eigenwavelengths in Fig. 2(a). The existence of two kinds of modes, i.e., the host modes and the ELM, is evident. While all the methods predict the same eigenwavelengths for the host modes, the incongruent predictions for the ELM allude to the criticality of the QHDM treatment. HW-HDM effectively causes electron spill-in and hence a blueshift of the ELM resonance by 95 nm. The LRA method, with no electron spill-out or spill-in effect, produces a blueshift of 31 nm. The induced current and electron density profiles of the ELM are plotted in logarithmic scale in Fig. 2(b). The common feature of these plots is the localization of the induced current and electron densities around the protrusion even though there is no inner physical boundary between the protrusion and host. Beyond the common feature, the QHDM analysis gives the most rational distributions by allowing the induced current to fade away beyond the geometry boundary. The electron density distributions exhibit even greater difference. Under LRA, the induced charge density only

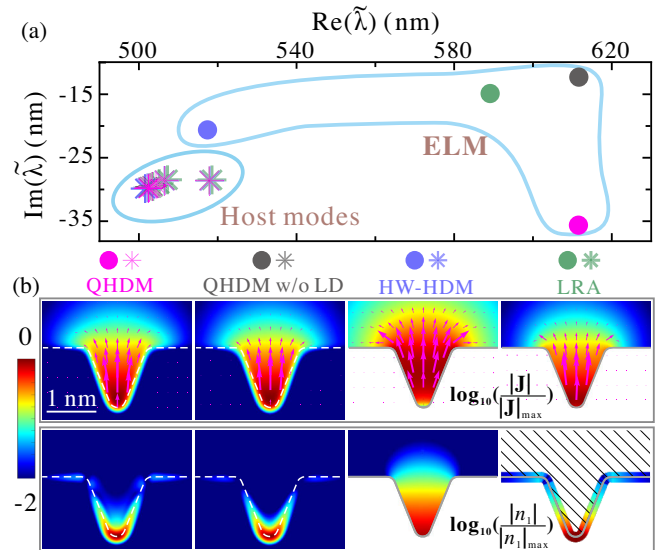


FIG. 2. (a) Calculated eigenwavelengths of the QNMs for the structure shown in Fig. 1(a) with $h_p = 1.2$ nm using four different approaches. The eigenwavelengths are grouped into two categories, i.e., host modes and ELM. (b) Distributions of the calculated current density $|\mathbf{J}|$ and electron density $|n_1|$ associated with the ELM in logarithmic scale.

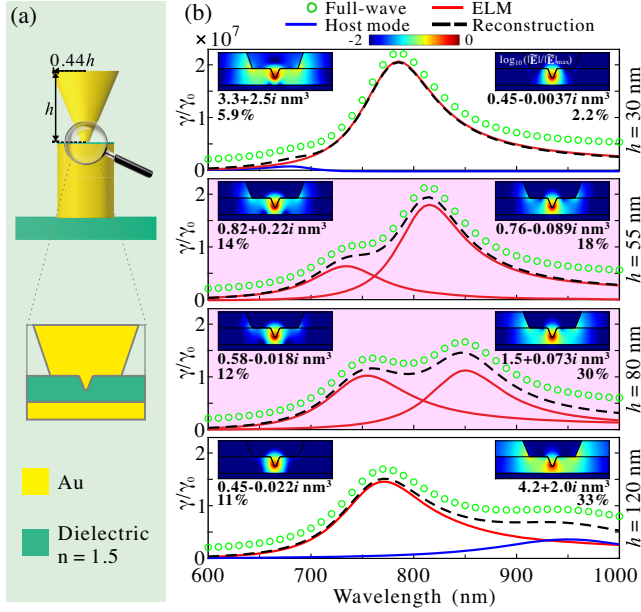


FIG. 3. (a) Schematic diagram of the composite antenna structure. (b) Calculated emission enhancement spectra for the antennas with $h = 30, 55, 80,$ and 120 nm. The full-wave results, separate modal contributions from the ELMs and host modes, and the reconstruction are plotted with green circles, solid, and black dashed traces, respectively. The insets display the mode profiles of the two QNMs with the mode volume and radiation efficiency indicated.

exists on the surface. In contrast, under HW-HDM, the electrons diffuse into the entire protrusion. The QHDM calculations reinstate the surface plasmon nature that the induced electrons reside in a thin layer and fade away (spill out) from the boundary. LD further causes charge diffusion in the protrusion, consistent with the diffusion interpretation [57]. With LD included, the quality factor of the ELM is reduced by 3 times as shown in Fig. 2(a). One learns from these responses that driving the current and electrons around the protrusion is the pivotal factor in forming the ELM. Indeed, the gap-plasmon mode enhanced by the lightning rod effect is associated with delocalized current and electron distributions [37].

Extreme light concentration and high radiation efficiency are two ends difficult to reconcile [22,58] due to LD and the huge mismatch between the mode size and free-space wavelength. Indeed, the radiative portions of the emission enhancement from the ELMs in Fig. 1(a) are barely over 0.001%. To solve the dilemma, we propose the idea of coupling the ELM with the host mode so that the radiation rate of the ELM can outpace or compete with LD. As sketched in Fig. 3(a), we explore the idea by designing a nanocone-cylinder antenna (characterized by its height h) as the host for the protrusion with $h_p = 1.2$ nm. The emission enhancement spectra are calculated and plotted with green circles in Fig. 3(b) for the nanocone with $h = 30, 55, 80,$ and 120 nm. Note that the mode interaction

here does not produce Fano-like resonances as in some recently studied metallodielectric hybrid structures [59] since necessary conditions are not met [60]. The spectra are also reconstructed with modal contributions [37] as indicated by the color-coded traces. The insets display the mode profiles of the two involved QNMs for each host antenna structure with the mode volume and radiation efficiency indicated. Induced current distributions additionally reveal their dipolar nature [37]. For $h = 30$ and 120 nm, the two QNMs are distantly separated in the spectra and the interaction is weak. For $h = 55$ and 80 nm, the interaction becomes strong and the ELM sacrifices a bit of confinement, whereas the host mode becomes extremely concentrated to around 1 nm^3 . Interestingly the radiation efficiencies of these hybridized ELMs are significantly boosted. Strikingly, for $h = 80$ nm, the radiation efficiency of the main-contributing ELM with a mode volume of 1.5 nm^3 reaches 30%. For $h = 55$ nm, the emission enhancement around 808 nm has a radiation efficiency of 18% and is contributed to vastly ($\sim 84\%$) by an ELM with the mode volume of only 0.78 nm^3 .

Efficient radiation from an ELM implies it could be accessible from the far field. To exploit this possibility, we launch a focused radially polarized beam [37,61] to illuminate the antenna structure shown in Fig. 3(b) with $h = 55$ nm. The calculated scattering and absorption spectra of the antenna with and without the protrusion are shown in Fig. 4(a). The effect of the protrusion is pronounced with both the scattering and absorption spectra split into two resonances corresponding to the ELMs. This suggests an efficient delivery of the far field optical energy into a tiny space. Figure 4(b) displays the distribution of the intensity enhancement with respect to the case without the antenna at the resonant wavelength of 808 nm. The far field

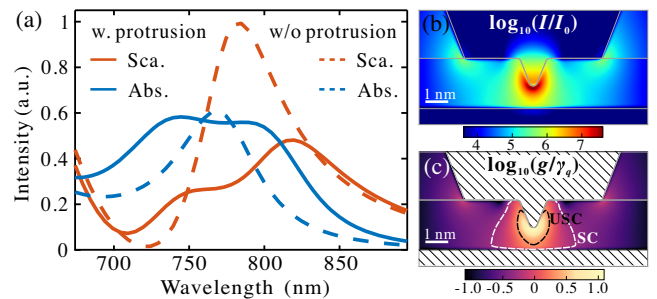


FIG. 4. (a) Calculated scattering (Sca.) and absorption (Abs.) spectra of antenna structure studied in Fig. 3(b) with $h = 55$ nm under the illumination of a focused radially polarized beam. Spectra without the protrusion are shown in dashed lines. (b) Light intensity enhancement in logarithmic scale for the far field excitation at 808 nm. (c) Atom-field coupling constant normalized by the ELM's relaxation rate in logarithmic scale. The white and black dashed contours demarcate the regions reaching strong (SC) and ultrastrong (USC) coupling regimes, respectively.

excitation is effectively concentrated to a volume of $\sim 1 \text{ nm}^3$ with an unprecedented enhancement up to 4×10^7 . In view of such ultrahigh enhancement, the weak excitation limit could be easily surpassed and our linearized treatment of QHDM may become insufficient due to the nonlinear effects [62–64]. For this case, we estimate the influence of the nonlinear effects on the linear response should be negligible for incident electric field with an amplitude below 1000 V/m [64]. An optical mode with about 1 nm^3 volume also promises an extremely strong coupling with a single emitter. The coupling strength with a dipolar emitter can be characterized by the coupling constant [24,65] $g = \sqrt{\gamma_0 \gamma_q \rho(\mathbf{r}, \omega_q)}/2$, with $\gamma_q = 74 \text{ meV}$ being the decay rate of the ELM at $\omega_q = 1.5 \text{ eV}$ and $\gamma_0 = (10 \text{ ns})^{-1}$ being the spontaneous decay rate of a typical emitter. The local density of states $\rho(\mathbf{r})$ can be approximated by the modal emission enhancement $f_{p,q}(\mathbf{r})$. Figure 4(c) maps the coupling constant. The white contour indicates the strong coupling threshold of $g = \gamma_q/2$ and the black contour denotes the ultrastrong coupling criterion of $g = 0.1\omega_q$ [66]. The calculated maximum coupling energy under the electric-dipole approximation reaches 790 meV . The ultrastrong coupling phenomena with single emitters have mainly been discussed in the microwave range [66] and now it seems possible with the ELMs at optical frequencies.

We have shown the robust existence of extremely localized modes around atomistic protrusions on a host nanoparticle. The predictions from our QHDM-based QNM analysis are reliable and tolerant to the changes of various approximations, including the von Weizsäcker parameter in T_w and correlation approximation [37]. Bright, extremely localized modes promise ultrafast light sources and huge enhancement of various low cross section processes at subnanometer scale, such as Raman scattering [20,21,67–71] and nonlinear phenomena [63]. Our findings should be extendable to other materials and geometries and underpin exciting new sciences, for instance, unlocking forbidden transitions [72] and atomic-scale photochemistry [73].

We gratefully acknowledge financial support from the National Natural Science Foundation of China (Grants No. 11874166 and No. 11604109).

*puzhang0702@hust.edu.cn

†xuewen_chen@hust.edu.cn

- [1] W. L. Barnes, A. Dereux, and T. W. Ebbesen, Surface plasmon subwavelength optics, *Nature (London)* **424**, 824 (2003).
 [2] J. A. Schuller, E. S. Barnard, W. Cai, Y. C. Jun, J. S. White, and M. L. Brongersma, Plasmonics for extreme light concentration and manipulation, *Nat. Mater.* **9**, 193 (2010).

- [3] A. F. Koenderink, A. Alù, and A. Polman, Nanophotonics: Shrinking light-based technology, *Science* **348**, 516 (2015).
 [4] L. Novotny and N. van Hulst, Antennas for light, *Nat. Photonics* **5**, 83 (2011).
 [5] H. T. Miyazaki and Y. Kurokawa, Squeezing Visible Light Waves into a 3-nm-Thick and 55-nm-Long Plasmon Cavity, *Phys. Rev. Lett.* **96**, 097401 (2006).
 [6] J. Gersten and A. Nitzan, Electromagnetic theory of enhanced Raman scattering by molecules adsorbed on rough surfaces, *J. Chem. Phys.* **73**, 3023 (1980).
 [7] M. I. Stockman, Nanofocusing of Optical Energy in Tapered Plasmonic Waveguides, *Phys. Rev. Lett.* **93**, 137404 (2004).
 [8] R. Gordon and A. Ahmed, Reaching the limits of enhancement in (sub)nanometer metal structures, *ACS Photonics* **5**, 4222 (2018).
 [9] J. Kern, S. Großmann, N. V. Tarakina, T. Häckel, M. Emmerling, M. Kamp, J.-S. Huang, P. Biagioni, J. C. Prangsma, and B. Hecht, Atomic-scale confinement of resonant optical fields, *Nano Lett.* **12**, 5504 (2012).
 [10] C. Ciraci, R. T. Hill, J. J. Mock, Y. Urzhumov, A. I. Fernández-Domínguez, S. A. Maier, J. B. Pendry, A. Chilkoti, and D. R. Smith, Probing the ultimate limits of plasmonic enhancement, *Science* **337**, 1072 (2012).
 [11] R. Chikkaraddy, B. de Nijs, F. Benz, S. J. Barrow, O. A. Scherman, E. Rosta, A. Demetriadou, P. Fox, O. Hess, and J. J. Baumberg, Single-molecule strong coupling at room temperature in plasmonic nanocavities, *Nature (London)* **535**, 127 (2016).
 [12] J. J. Baumberg, J. Aizpurua, M. H. Mikkelsen, and D. R. Smith, Extreme nanophotonics from ultrathin metallic gaps, *Nat. Mater.* **18**, 668 (2019).
 [13] I. Epstein, D. Alcaraz, Z. Huang, V.-V. Pusapati, J.-P. Hugonin, A. Kumar, X. M. Deputy, T. Khodkov, T. G. Rappoport, J.-Y. Hong, N. M. R. Peres, J. Kong, D. R. Smith, and F. H. L. Koppens, Far-field excitation of single graphene plasmon cavities with ultracompressed mode volumes, *Science* **368**, 1219 (2020).
 [14] F. Benz, M. K. Schmidt, A. Dreismann, R. Chikkaraddy, Y. Zhang, A. Demetriadou, C. Carnegie, H. Ohadi, B. de Nijs, R. Esteban, J. Aizpurua, and J. J. Baumberg, Single-molecule optomechanics in “picocavities”, *Science* **354**, 726 (2016).
 [15] B. Yang, G. Chen, A. Ghafoor, Y. Zhang, Y. Zhang, Y. Zhang, Y. Luo, J. Yang, V. Sandoghdar, J. Aizpurua, Z. Dong, and J. G. Hou, Sub-nanometre resolution in single-molecule photoluminescence imaging, *Nat. Photonics* **14**, 693 (2020).
 [16] M. Barbry, P. Koval, F. Marchesin, R. Esteban, A. G. Borisov, J. Aizpurua, and D. Sánchez-Portal, Atomistic near-field nanoplasmonics: Reaching Atomic-scale resolution in nanooptics, *Nano Lett.* **15**, 3410 (2015).
 [17] S. Trautmann, J. Aizpurua, I. Götz, A. Undisz, J. Dellith, H. Schneidewind, M. Rettenmayr, and V. Deckert, A classical description of subnanometer resolution by atomic features in metallic structures, *Nanoscale* **9**, 391 (2017).
 [18] M. Urbieta, M. Barbry, Y. Zhang, P. Koval, D. Sánchez-Portal, N. Zabala, and J. Aizpurua, Atomic-scale lightning rod effect in plasmonic picocavities: A classical view to a quantum effect, *ACS Nano* **12**, 585 (2018).

- [19] H. Ohnishi, Y. Kondo, and K. Takayanagi, Quantized conductance through individual rows of suspended gold atoms, *Nature (London)* **395**, 780 (1998).
- [20] R. Zhang, Y. Zhang, Z. C. Dong, S. Jiang, C. Zhang, L. G. Chen, L. Zhang, Y. Liao, J. Aizpurua, Y. Luo, J. L. Yang, and J. G. Hou, Chemical mapping of a single molecule by plasmon-enhanced Raman scattering, *Nature (London)* **498**, 82 (2013).
- [21] J. Lee, K. T. Crampton, N. Tallarida, and V. A. Apkarian, Visualizing vibrational normal modes of a single molecule with atomically confined light, *Nature (London)* **568**, 78 (2019).
- [22] J. Khurgin, W.-Y. Tsai, D. P. Tsai, and G. Sun, Landau damping and limit to field confinement and enhancement in plasmonic dimers, *ACS Photonics* **4**, 2871 (2017).
- [23] S. Raza, S. I. Bozhevolnyi, M. Wubs, and N. A. Mortensen, Nonlocal optical response in metallic nanostructures, *J. Phys. Condens. Matter* **27**, 183204 (2015).
- [24] S. Haroche and J.-M. Raimond, *Exploring the Quantum: Atoms, Cavities, and Photons* (Oxford University Press, New York, 2006).
- [25] A. F. Koenderink, On the use of Purcell factors for plasmon antennas, *Opt. Lett.* **35**, 4208 (2010).
- [26] C. Sauvan, J. P. Hugonin, I. S. Maksymov, and P. Lalanne, Theory of the Spontaneous Optical Emission of Nanosize Photonic and Plasmon Resonators, *Phys. Rev. Lett.* **110**, 237401 (2013).
- [27] P. Lalanne, W. Yan, K. Vynck, C. Sauvan, and J.-P. Hugonin, Modeling electromagnetic resonators using quasinormal modes, *Laser Photonics Rev.* **12**, 1700113 (2018).
- [28] S. V. Lobanov, W. Langbein, and E. A. Muljarov, Resonant-state expansion of three-dimensional open optical systems: Light scattering, *Phys. Rev. A* **98**, 033820 (2018).
- [29] P. T. Kristensen, K. Herrmann, F. Intravaia, and K. Busch, Modeling electromagnetic resonators using quasinormal modes, *Adv. Opt. Photonics* **12**, 612 (2020).
- [30] M. K. Dezfouli, C. Tserkezis, N. A. Mortensen, and S. Hughes, Nonlocal quasinormal modes for arbitrarily shaped three-dimensional plasmonic resonators, *Optica* **4**, 1503 (2017).
- [31] F. Binkowski, L. Zschiedrich, M. Hammerschmidt, and S. Burger, Modal analysis for nanoplasmonics with nonlocal material properties, *Phys. Rev. B* **100**, 155406 (2019).
- [32] J. A. Scholl, A. L. Koh, and J. A. Dionne, Quantum plasmon resonances of individual metallic nanoparticles, *Nature (London)* **483**, 421 (2012).
- [33] G. Toscano, J. Straubel, A. Kwiatkowski, C. Rockstuhl, F. Evers, H. Xu, N. A. Mortensen, and M. Wubs, Resonance shifts and spill-out effects in self-consistent hydrodynamic nanoplasmonics, *Nat. Commun.* **6**, 7132 (2015).
- [34] J. Zuloaga, E. Prodan, and P. Nordlander, Quantum description of the plasmon resonances of a nanoparticle dimer, *Nano Lett.* **9**, 887 (2009).
- [35] K. Ding and C. T. Chan, Plasmonic modes of polygonal rods calculated using a quantum hydrodynamics method, *Phys. Rev. B* **96**, 125134 (2017).
- [36] C. Ciraci, Current-dependent potential for nonlocal absorption in quantum hydrodynamic theory, *Phys. Rev. B* **95**, 245434 (2017).
- [37] See Supplemental Material at <http://link.aps.org/supplemental/10.1103/PhysRevLett.126.257401> for additional details, including a self-contained introduction to the QHDM-QNM theory, full derivations of the main results, and an extended discussion of the QHDM computation and the ELMs, which includes Refs. [38–52].
- [38] W. Yan, Hydrodynamic theory for quantum plasmonics: Linear-response dynamics of the inhomogeneous electron gas, *Phys. Rev. B* **91**, 115416 (2015).
- [39] M. Kupresak, X. Zheng, G. A. E. Vandenbosch, and V. V. Moshchalkov, Comparison of hydrodynamic models for the electromagnetic nonlocal response of nanoparticles, *Adv. Theory Simul.* **1**, 1800076 (2018).
- [40] J. Hurst, P. M. Oppeneer, G. Manfredi, and P.-A. Hervieux, Magnetic moment generation in small gold nanoparticles via the plasmonic inverse Faraday effect, *Phys. Rev. B* **98**, 134439 (2018).
- [41] A. Raman and S. Fan, Photonic Band Structure of Dispersive Metamaterials Formulated as a Hermitian Eigenvalue Problem, *Phys. Rev. Lett.* **104**, 087401 (2010).
- [42] W. Yan, R. Faggiani, and P. Lalanne, Rigorous modal analysis of plasmonic nanoresonators, *Phys. Rev. B* **97**, 205422 (2018).
- [43] G. Kewes, F. Binkowski, S. Burger, L. Zschiedrich, and O. Benson, Heuristic modeling of strong coupling in plasmonic resonators, *ACS Photonics* **5**, 4089 (2018).
- [44] M. Scalora, M. A. Vincenti, D. de Ceglia, and J. W. Haus, Nonlocal and quantum-tunneling contributions to harmonic generation in nanostructures: Electron-cloud-screening effects, *Phys. Rev. A* **90**, 013831 (2014).
- [45] D. R. Lide, *CRC Handbook of Chemistry and Physics*, 87th ed. (CRC Press, Boca Raton, FL, 2006).
- [46] F. Binkowski, F. Betz, R. Colom, M. Hammerschmidt, L. Zschiedrich, and S. Burger, Quasinormal mode expansion of optical far-field quantities, *Phys. Rev. B* **102**, 035432 (2020).
- [47] S. Quabis, R. Dorn, M. Eberler, O. Glöckl, and G. Leuchs, The focus of light – theoretical calculation and experimental tomographic reconstruction, *Appl. Phys. B* **72**, 109 (2001).
- [48] X.-W. Chen, V. Sandoghdar, and M. Agio, Nanofocusing radially-polarized beams for high-throughput funneling of optical energy to the near field, *Opt. Express* **18**, 10878 (2010).
- [49] R. G. Parr and W. Yang, *Density-Functional Theory of Atoms and Molecules* (Oxford University Press, New York, 1995).
- [50] J. P. Perdew and A. Zunger, Self-interaction correction to density-functional approximations for many-electron systems, *Phys. Rev. B* **23**, 5048 (1981).
- [51] O. Gunnarsson and B. I. Lundqvist, Exchange and correlation in atoms, molecules, and solids by the spin-density-functional formalism, *Phys. Rev. B* **13**, 4274 (1976).
- [52] E. Wigner, On the interaction of electrons in metals, *Phys. Rev.* **46**, 1002 (1934).
- [53] Q. Bai, M. Perrin, C. Sauvan, J.-P. Hugonin, and P. Lalanne, Efficient and intuitive method for the analysis of light scattering by a resonant nanostructure, *Opt. Express* **21**, 27371 (2013).
- [54] P. T. Kristensen, C. V. Vlack, and S. Hughes, Generalized effective mode volume for leaky optical cavities, *Opt. Lett.* **37**, 1649 (2012).

- [55] E. A. Muljarov and W. Langbein, Exact mode volume and Purcell factor of open optical systems, *Phys. Rev. B* **94**, 235438 (2016).
- [56] L. Zschiedrich, F. Binkowski, N. Nikolay, O. Benson, G. Kewes, and S. Burger, Riesz-projection-based theory of light-matter interaction in dispersive nanoresonators, *Phys. Rev. A* **98**, 043806 (2018).
- [57] N. A. Mortensen, S. Raza, M. Wubs, T. Søndergaard, and S. I. Bozhevolnyi, A generalized non-local optical response theory for plasmonic nanostructures, *Nat. Commun.* **5**, 3809 (2014).
- [58] J. T. Hugall, A. Singh, and N. F. van Hulst, Plasmonic cavity coupling, *ACS Photonics* **5**, 43 (2018).
- [59] S. Franke, S. Hughes, M. K. Dezfouli, P. T. Kristensen, K. Busch, A. Knorr, and M. Richter, Quantization of Quasinormal Modes for Open Cavities and Plasmonic Cavity Quantum Electrodynamics, *Phys. Rev. Lett.* **122**, 213901 (2019).
- [60] B. Gallinet and O. J. F. Martin, Influence of electromagnetic interactions on the line shape of plasmonic fano resonances, *ACS Nano* **5**, 8999 (2011).
- [61] R. Dorn, S. Quabis, and G. Leuchs, Sharper Focus for a Radially Polarized Light Beam, *Phys. Rev. Lett.* **91**, 233901 (2003).
- [62] A. Hille, M. Moferdt, C. Wolff, C. Matyssek, R. Rodríguez-Oliveros, C. Prohm, J. Niegemann, S. Grafstrøm, L. M. Eng, and K. Busch, Second harmonic generation from metal nano-particle resonators: Numerical analysis on the basis of the hydrodynamic Drude model, *J. Phys. Chem. C* **120**, 1163 (2016).
- [63] A. V. Krasavin, P. Ginzburg, G. A. Wurtz, and A. V. Zayats, Nonlocality-driven supercontinuum white light generation in plasmonic nanostructures, *Nat. Commun.* **7**, 11497 (2016).
- [64] M. Khalid and C. Ciraci, Enhancing second-harmonic generation with electron spill-out at metallic surfaces, *Commun. Phys.* **3**, 214 (2020).
- [65] F. Marquier, C. Sauvan, and J.-J. Greffet, Revisiting quantum optics with surface plasmons and plasmonic resonators, *ACS Photonics* **4**, 2091 (2017).
- [66] A. F. Kockum, A. Miranowicz, S. De Liberato, S. Savasta, and F. Nori, Ultrastrong coupling between light and matter, *Nat. Rev. Phys.* **1**, 19 (2019).
- [67] H. Xu, E. J. Bjerneld, M. Käll, and L. Börjesson, Spectroscopy of Single Hemoglobin Molecules by Surface Enhanced Raman Scattering, *Phys. Rev. Lett.* **83**, 4357 (1999).
- [68] E. C. Le Ru, E. Blackie, M. Meyer, and P. G. Etchegoin, Surface enhanced Raman scattering enhancement factors: A comprehensive study, *J. Phys. Chem. C* **111**, 13794 (2007).
- [69] P. Liu, D. V. Chulhai, and L. Jensen, Single-molecule imaging using atomistic near-field tip-enhanced Raman spectroscopy, *ACS Nano* **11**, 5094 (2017).
- [70] P. L. Stiles, J. A. Dieringer, N. C. Shah, and R. P. Van Duyne, Surface-enhanced Raman spectroscopy, *Annu. Rev. Anal. Chem.* **1**, 601 (2008).
- [71] Y. Yu, T.-H. Xiao, Y. Wu, W. Li, Q.-G. Zeng, L. Long, and Z.-Y. Li, Roadmap for single-molecule surface-enhanced Raman spectroscopy, *Adv. Opt. Photonics* **2**, 1 (2020).
- [72] N. Rivera, I. Kaminer, B. Zhen, J. D. Joannopoulos, and M. Soljačić, Shrinking light to allow forbidden transitions on the atomic scale, *Science* **353**, 263 (2016).
- [73] M. Kamp, B. de Nijs, N. Kongsuwan, M. Saba, R. Chikkaraddy, C. A. Readman, W. M. Deacon, J. Griffiths, S. J. Barrow, O. S. Ojambati, D. Wright, J. Huang, O. Hess, O. A. Scherman, and J. J. Baumberg, Cascaded nanooptics to probe microsecond atomic-scale phenomena, *Proc. Natl. Acad. Sci. U.S.A.* **117**, 14819 (2020).